Engineering Analysis with Boundary Elements 147 (2023) 171–180

Contents lists available at ScienceDirect

Engineering Analysis with Boundary Elements

journal homepage: www.elsevier.com/locate/enganabound

A fast direct boundary element method for 3D acoustic problems based on hierarchical matrices

Ruoyan Li [a,b], Yijun Liu [a,*], Wenjing Ye [b]

[a] Department of Mechanics and Aerospace Engineering, Southern University of Science and Technology, Shenzhen, PR China
[b] Department of Mechanical and Aerospace Engineering, The Hong Kong University of Science and Technology, Hong Kong, PR China

ARTICLE INFO

Keywords:
Boundary element method
Fast direct solver
Hierarchical matrices
3-D acoustic wave problems

ABSTRACT

The boundary element method (BEM) for acoustic problems is a numerical method based on solving the discretized boundary integral equation (BIE) corresponding to the Helmholtz equation. A fast direct BEM for 3D acoustic problems is proposed in this paper, which is more suitable for broadband acoustic simulation of complex structures, such as in the design and analysis of acoustic metamaterials. The main idea of the fast direct solver is based on the hierarchical off-diagonal low-rank (HODLR) matrix, randomized interpolative decomposition and fast matrix inversion formula. Several numerical examples in solving both interior and exterior acoustic problems are presented in this paper, including radiation and scattering problems with distributed and complex structures. The numerical results show that the same level of accuracy and higher computational efficiency can be achieved by using this fast direct BEM compared with the conventional direct BEM.

The second and third authors (Liu and Ye) would like to dedicate this paper to Professor Subrata Mukherjee who had enormous influences on their academic lives and research work on the BEM.

1. Introduction

The boundary element method (BEM) is a numerical method based on solving the boundary integral equation (BIE) for a given problem. In general, the BEM has the advantages of boundary discretization only and higher accuracy compared with other numerical methods. It is particularly suitable for solving wave propagation problems in infinite domains, such as an acoustic wave problem in an open space. However, there have been two critical issues associated with the development of the acoustic BEM: the uniqueness of the BEM solutions for exterior domains due to the fictitious eigenfrequency, and the computational efficiency of the BEM solutions due to its nonsymmetric and fully-populated matrices.

The Burton-Miller BIE formulation [1,2], using a linear combination of the conventional BIE and derivative BIE, has been proved to be the most stable formulation for solving exterior acoustic wave problems. This combined BIE formulation can be applied to overcame the fictitious eigenfrequency problem in exterior wave problems when the wavenumber is a real number [3], as well as the thin-shape breakdown problems [4,5].

To improve the computational efficiency of the acoustic BEM, several types of fast solution methods have been developed and applied in the acoustic BEM in the last three decades. The most popular one is the fast multipole method (FMM) for Helmholtz equation proposed by Rokhlin and Greengard [6,7]. The basic procedure of FMM is to hierarchically group elements into cells in a tree structure, evaluate kernel integration with multipole expansions, local expansions and translations, and compute the matrix-vector multiplication using an iterative solver to update the solution. Another widely studied fast solution method is the adaptive cross approximation (ACA) BEM. It is also based on using an iterative solver and the hierarchical matrix ($\mathcal{H}$-matrix) introduced by Hackbusch [8]. ACA is used for the approximation of low-rank submatrices after hierarchical division of dense coefficient matrices. The ACA-BEM is kernel-independent, relies only on the algebra of the coefficient matrix. More details of the two approaches can be found in several studies [9–12] for the FMM-BEM and some works [13–16] for the ACA-BEM.

Both the FMM-BEM and ACA-BEM are methods utilizing iterative solvers, such as the commonly used generalized minimal residual method (GMRES) [17]. One issue with an iterative solver is the convergence of solutions. It is well-known that for acoustic problems, large wavenumber and complex geometry often lead to an

* Corresponding author.
E-mail address: liuyj3@sustech.edu.cn (Y. Liu).

https://doi.org/10.1016/j.enganabound.2022.11.035
Received 8 October 2022; Received in revised form 16 November 2022; Accepted 29 November 2022
Available online 14 December 2022

ill-conditioned linear system of equations, resulting in a large number of iterations before the solution can converge to a specified accuracy. One way to accelerate the convergence is to use a good preconditioner, but the efficiency and adaptability of the preconditioner can vary from case to case.

A more recent approach in fast solution methods is to solve the BEM system of equations directly with the help of the concept related to the $\mathscr{H}$-matrix and approximation. This is the so called fast direct BEM which is based mainly on using $\mathscr{H}$-matrices, low-rank approximations and decompositions, and fast inverse algorithms on submatrices to recursively obtain the solution of the BEM system. Many types of the $\mathscr{H}$-matrix with different complexity are used to construct the fast direct solver, such as the hierarchically semiseparable (HSS) matrix [18], the hierarchical off-diagonal low-rank (HODLR) matrix [19], and the $\mathscr{H}$-matrix [20]. A HODLR matrix can be represented by multiplication of a diagonal matrix and several block diagonal matrices, where all off-diagonal blocks are low-rank approximated, and can be inverted by the Sherman–Morrison–Woodbury formula efficiently. Because of this characteristic and the fact that the solution time is predictable for a given sized problem, the fast direct BEM solver has gained popularity in recent years. For example, Greengard's group has worked on HODLR based fast direct BEM for 2D acoustic and electromagnetic wave scattering problems [21,22]; and Martinsson's group studied the fast and accurate compression strategies for applying the HODLR matrix [23,24]. The HODLR based fast direct BEM and accurate matrix approximation method were applied for solving 3D potential problems [25], as well as the isogeometric BEM (IGABEM) [26].

In this paper, we present a fast direct solver based on the HODLR matrix and interpolative decomposition (ID) approximation strategy for solving 3D acoustic wave propagation problems. The following of the paper is organized as follows: in Section 2, the BIE formulation for solving acoustic wave problems is reviewed; in Section 3, the applied HODLR matrix and interpolative decomposition approximation are presented; in Section 4, the algorithms used in the fast direct BEM solver are illustrated; in Section 5, a few numerical examples are presented to demonstrate the accuracy and efficiency of the developed fast direct BEM solver; and in Section 6, some discussions on the method are provided to conclude the paper.

2. BIE formulation

Consider the Helmholtz equation, which is the governing equation for acoustic wave problems in the frequency domain, in domain E (either finite or infinite):

$$\nabla^2\phi + k^2\phi + Q\delta(\mathbf{x},\mathbf{x}_Q) = 0, \qquad \forall \mathbf{x} \in E \tag{1}$$

where ϕ is the complex acoustic pressure at location $\mathbf{x}$, k is the wavenumber, and $Q\delta(x, x_Q)$ represents a point sound source at point $\mathbf{x}_Q$ inside E, Q is amplitude of source, and $\delta(\mathbf{x}, \mathbf{x}_Q)$ is the Dirac delta function. And $k = \omega/c$ with ω being the circular frequency and c being the speed of sound in the acoustic medium E.

There are three types of boundary conditions on the boundary S of domain E:

1) Sound pressure is given:

$$\phi = \overline{\phi}; \tag{2}$$

2) Particle velocity is given:

$$q \equiv \frac{\partial\phi}{\partial n} = \overline{q} = i\omega\rho v_n; \tag{3}$$

3) Impedance of the surface is given:

$$\phi = Zv_n; \tag{4}$$

where the overbar symbol indicates a given value, ρ is the density of acoustic medium, v_n is the normal velocity of the acoustic medium, and Z is the specific acoustic impedance.

Applying the Green's second identity for two continuous functions u and v:

$$\int_V \left[u\nabla^2 v - v\nabla^2 u\right] dE = \int_S \left[u\frac{\partial v}{\partial n} - v\frac{\partial u}{\partial n}\right] dS, \tag{5}$$

and the Sommerfeld radiation condition for an infinite domain problem:

$$\lim_{R\to\infty}\left[R\left|\frac{\partial\phi}{\partial R} - ik\phi\right|\right] = 0, \tag{6}$$

one can derive the conventional BIE (CBIE) as:

$$c(\mathbf{x})\phi(\mathbf{x}) = \int_S [G(\mathbf{x},\mathbf{y},\omega)q(\mathbf{y}) - F(\mathbf{x},\mathbf{y},\omega)\phi(\mathbf{y})]dS(\mathbf{y}) + \phi^I(\mathbf{x}) + QG(\mathbf{x},\mathbf{x}_Q,\omega), \tag{7}$$

where the incident wave term $\phi^I(\mathbf{x})$ is not present for radiation problem; $c(\mathbf{x})$ is a constant, and$G$ and F are the fundamental solution for 3D acoustic wave problem [2]:

$$c(x) = \begin{cases} 1, \ \forall x \in V, \\ 1/2, \ \forall x \in S(smooth), \\ 0, \ \forall x \notin V \cup S; \end{cases} \tag{8}$$

$$G(\mathbf{x},\mathbf{y},\omega) = \frac{1}{4\pi r}e^{ikr}; \tag{9}$$

$$F(\mathbf{x},\mathbf{y},\omega) \equiv \frac{\partial G(\mathbf{x},\mathbf{y},\omega)}{\partial n(\mathbf{y})} = \frac{1}{4\pi r^2}(ikr-1)r_{,j}n_j(\mathbf{y})e^{ikr}; \tag{10}$$

in which r is the distance from a source point $\mathbf{x}$ to a field point $\mathbf{y}$. Solving the CBIE with given boundary conditions, one can obtain all the unknowns on boundary S, which can then be used to compute the desired pressure values at points in domain E. However, the CBIE is flawed when used to solve an exterior problem at a fictitious eigenfrequency or in a domain with thin structures [1,2,4,5]. A dual formulation consisting of the CBIE and its normal derivative proposed by Burton and Miller [1] is an effective approach for solving both of the problems [5].

Taking the derivate of the CBIE with respected to the normal direction at point $\mathbf{x}$ and let $\mathbf{x}$ approach to boundary S, one obtains the so-called hypersingular BIE (HBIE) as:

$$\widetilde{c}(\mathbf{x})q(\mathbf{x}) = \int_S [K(\mathbf{x},\mathbf{y},\omega)q(\mathbf{y}) - H(\mathbf{x},\mathbf{y},\omega)\phi(\mathbf{y})]dS(\mathbf{y}) + q^I(\mathbf{x}) + QK(\mathbf{x},\mathbf{x}_Q,\omega), \quad \forall \mathbf{x} \in S, \tag{11}$$

where $\widetilde{c}(\mathbf{x}) = 1/2$ if S is smooth around $\mathbf{x}$, $q^I(\mathbf{x})$ is the normal derivative of incident wave $\phi^I(\mathbf{x})$ and the two new kernels are [9]:

$$K(\mathbf{x},\mathbf{y},\omega) \equiv \frac{\partial G(\mathbf{x},\mathbf{y},\omega)}{\partial n(\mathbf{x})} = -\frac{1}{4\pi r^2}(ikr-1)r_{,j}n_j(\mathbf{x})e^{ikr}, \tag{12}$$

$$H(x,y,\omega) \equiv \frac{\partial F(x,y,\omega)}{\partial n(x)} = \frac{1}{4\pi r^3}\left\{(1-ikr)n_j(y) + \left[k^2r^2 - 3(1-ikr)\right]r_{,j}r_{,l}n_l(y)\right\}n_j(x)e^{ikr}. \tag{13}$$

Then, the Burton-Miller (B-M) formulation, which is also called dual BIE formulation, can be written symbolically as:

$$\text{CBIE} + \beta\,\text{HBIE} = 0 \tag{14}$$

where β is a coupling coefficient. In this paper, $\beta = -ih$ is used. The strongly singular integrals F and K, and the hypersingular integral H, can be dealt with using the regularized or weakly-singular forms of the CBIE and HBIE with the help of the corresponding static kernels for the potential problem [9,27].

Solving the BIEs with the BEM using, for example, constant boundary elements, the discretized equation can be written in the following form:

$$\mathbf{A}\lambda = \mathbf{b} \tag{15}$$

where $\mathbf{A}$ is the BEM system matrix with complex coefficients, $\mathbf{b}$ is the known vector, and λ is the vector of all unknowns on the boundary elements. In general, solving this system of equations with N unknowns using a conventional direct solver requires the complexity of $O(N^2)$ for memory storage and $O(N^3)$ for solution. In this work, a fast direct solver is developed based on hierarchical matrices in order to reduce both the complexity in memory storage and solution time.

3. HODLR matrix and randomized interpolative decomposition

The $\mathscr{H}$-matrix is a large family of hierarchically divided matrices (see, for example, Ambikasaran's [28] paper for discussions on the classification). In the present work, the hierarchical off-diagonal low-rank (HODLR) matrix, which is one type of the $\mathscr{H}$-matrices, is applied to construct the fast direct solver for solving the BEM system of equations. The basic idea of the HODLR matrix is to divide the matrix into a hierarchical form and approximate all the off-diagonal low-rank submatrices. For example, for a fully populated matrix $\mathbf{K}$, the decomposition process can be represented by:

$$\mathbf{K} \approx \begin{bmatrix} \mathbf{K}_1^1 & \mathbf{U}_1^1\mathbf{V}_1^1 \\ \mathbf{U}_2^1\mathbf{V}_2^1 & \mathbf{K}_2^1 \end{bmatrix} \approx \begin{bmatrix} \begin{bmatrix} \mathbf{K}_1^2 & \mathbf{U}_1^2\mathbf{V}_1^2 \\ \mathbf{U}_2^2\mathbf{V}_2^2 & \mathbf{K}_2^2 \end{bmatrix} & \mathbf{U}_1^1\mathbf{V}_1^1 \\ \mathbf{U}_2^1\mathbf{V}_2^1 & \begin{bmatrix} \mathbf{K}_3^2 & \mathbf{U}_3^2\mathbf{V}_3^2 \\ \mathbf{U}_4^2\mathbf{V}_4^2 & \mathbf{K}_4^2 \end{bmatrix} \end{bmatrix} \approx \cdots$$

$$\approx \begin{bmatrix} \begin{bmatrix} \mathbf{K}_1^{l_\Pi} & \mathbf{U}_1^{l_\Pi}\mathbf{V}_1^{l_\Pi} \\ \mathbf{U}_2^{l_\Pi}\mathbf{V}_2^{l_\Pi} & \mathbf{K}_2^{l_\Pi} \end{bmatrix} & \mathbf{U}_1^{l_\Pi-1}\mathbf{V}_1^{l_\Pi-1} & \cdots & \cdots \\ \mathbf{U}_2^{l_\Pi-1}\mathbf{V}_2^{l_\Pi-1} & \begin{bmatrix} \mathbf{K}_3^{l_\Pi} & \mathbf{U}_3^{l_\Pi}\mathbf{V}_3^{l_\Pi} \\ \mathbf{U}_4^{l_\Pi}\mathbf{V}_4^{l_\Pi} & \mathbf{K}_4^{l_\Pi} \end{bmatrix} & \cdots & \cdots \\ \vdots & \vdots & \ddots & \cdots \\ \vdots & \vdots & \vdots & \begin{bmatrix} \mathbf{K}_{2^{l_\Pi}-1}^{l_\Pi} & \mathbf{U}_{2^{l_\Pi}-1}^{l_\Pi}\mathbf{V}_{2^{l_\Pi}-1}^{l_\Pi} \\ \mathbf{U}_{2^{l_\Pi}}^{l_\Pi}\mathbf{V}_{2^{l_\Pi}}^{l_\Pi} & \mathbf{K}_{2^{l_\Pi}}^{l_\Pi} \end{bmatrix} \end{bmatrix} \tag{16}$$

Eq. (16) can also be written as $\mathbf{K} \approx \mathbf{K}^1 \approx \mathbf{K}^2 \approx \cdots \approx \mathbf{K}^{l_\Pi}$ following the order shown in the equation, where the superscript l_Π indicates the level of HODLR matrix. $\mathbf{K}_i^{l_\Pi}$ indicates the i-th diagonal submatrix in the l_Π-level HODLR matrix $\mathbf{K}^{l_\Pi}$, and the corresponding off-diagonal submatrix is approximated into the multiplication of matrices $\mathrm{U}_i^{l_\Pi}$ and $\mathrm{V}_i^{l_\Pi}$. Any diagonal matrix $\mathbf{K}_i^l$ expect at the lowest level can be further expressed as:

$$\mathbf{K}_i^l = \begin{bmatrix} \mathbf{K}_{2i-1}^l & \mathbf{U}_{2i-1}^l\mathbf{V}_{2i-1}^l \\ \mathbf{U}_{2i}^l\mathbf{V}_{2i}^l & \mathbf{K}_{2i}^l \end{bmatrix} \tag{17}$$

where $i = 1, 2, 3, \cdots, 2^{l-1}$. Assume the dimensions of square matrix $\mathbf{K}_{2i-1}^l$ and $\mathbf{K}_{2i}^l$ are N_{2i-1}^l and N_{2i}^l, and those of the rectangular matrices $\mathbf{U}_{2i-1}^l$ and $\mathbf{U}_{2i}^l$ are $N_{2i-1}^l \times p_{2i-1}^l$ and $N_{2i}^l \times p_{2i}^l$ matrices, $\mathbf{V}_{2i-1}^l$ and $\mathbf{V}_{2i}^l$ are $p_{2i-1}^l \times N_{2i}^l$ and $p_{2i}^l \times N_{2i-1}^l$ matrices. In general, p is usually much smaller than the corresponding N, and N_{2i-1}^l is not necessarily equal to N_{2i}^l.

The HODLR matrix $\mathbf{K}^{l_\Pi}$ can be factorized as a multiplication of a sequence of matrices. For example, let $\mathbf{K}$ to be divided into the $\mathbf{K}^2$ form, which can be factorized as follows:

$$\mathbf{K}^2 = \begin{bmatrix} \begin{bmatrix} \mathbf{K}_1^2 & \mathbf{U}_1^2\mathbf{V}_1^2 \\ \mathbf{U}_2^2\mathbf{V}_2^2 & \mathbf{K}_2^2 \end{bmatrix} & \mathbf{U}_1^1\mathbf{V}_1^1 \\ \mathbf{U}_2^1\mathbf{V}_2^1 & \begin{bmatrix} \mathbf{K}_3^2 & \mathbf{U}_3^2\mathbf{V}_3^2 \\ \mathbf{U}_4^2\mathbf{V}_4^2 & \mathbf{K}_4^2 \end{bmatrix} \end{bmatrix}$$

$$= \begin{bmatrix} \mathbf{K}_1^2 & & & \\ & \mathbf{K}_2^2 & & \\ & & \mathbf{K}_3^2 & \\ & & & \mathbf{K}_4^2 \end{bmatrix} \begin{bmatrix} \begin{bmatrix} \mathbf{I} & {}^*\mathbf{U}_1^2\mathbf{V}_1^2 \\ {}^*\mathbf{U}_2^2\mathbf{V}_2^2 & \mathbf{I} \end{bmatrix} & {}^*\mathbf{U}_1^1\mathbf{V}_1^1 \\ {}^*\mathbf{U}_2^1\mathbf{V}_2^1 & \begin{bmatrix} \mathbf{I} & {}^*\mathbf{U}_3^2\mathbf{V}_3^2 \\ {}^*\mathbf{U}_4^2\mathbf{V}_4^2 & \mathbf{I} \end{bmatrix} \end{bmatrix} = \mathbf{K}_2 \begin{bmatrix} {}^*\mathbf{K}_1^1 & {}^*\mathbf{U}_1^1\mathbf{V}_1^1 \\ {}^*\mathbf{U}_2^1\mathbf{V}_2^1 & {}^*\mathbf{K}_2^1 \end{bmatrix}$$

$$= \mathbf{K}_2 \begin{bmatrix} {}^*\mathbf{K}_1^1 & \\ & {}^*\mathbf{K}_2^1 \end{bmatrix} \begin{bmatrix} \mathbf{I} & {}^*\mathbf{U}_1^1\mathbf{V}_1^1 \\ {}^*\mathbf{U}_2^1\mathbf{V}_2^1 & \mathbf{I} \end{bmatrix} = \mathbf{K}_2\mathbf{K}_1 \begin{bmatrix} \mathbf{I} & {}^*\mathbf{U}_1^1\mathbf{V}_1^1 \\ {}^*\mathbf{U}_2^1\mathbf{V}_2^1 & \mathbf{I} \end{bmatrix} = \mathbf{K}_2\mathbf{K}_1\mathbf{K}_0 \tag{18}$$

In general, the factorization of $\mathbf{K}^{l_\Pi}$ is $\mathbf{K}^{l_\Pi} = \mathbf{K}_{l_\Pi}\mathbf{K}_{l_\Pi-1}\ldots\mathbf{K}_0$, where $\mathbf{K}_{l_\Pi}$ is a diagonal matrix, and $\mathbf{K}_{l_\Pi-1},\ldots\mathbf{K}_1$ are block diagonal matrices with the block format as $\mathbf{K}_0$. $\mathbf{K}_{l_\Pi}$ can be easily inverted. And for any diagonal block ${}^*\mathbf{K}_i^l$ in $\mathbf{K}_l$ (l=0,1,…,l_Π−1 and i= 1, 2, ⋯, 2^l), one has:

$${}^*\mathbf{K}_i^l = \begin{bmatrix} \mathbf{I} & {}^*\mathbf{U}_{2i-1}^{l+1}\mathbf{V}_{2i-1}^{l+1} \\ {}^*\mathbf{U}_{2i}^{l+1}\mathbf{V}_{2i}^{l+1} & \mathbf{I} \end{bmatrix} = \mathbf{I} + \begin{bmatrix} {}^*\mathbf{U}_{2i-1}^{l+1} & \mathbf{0} \\ \mathbf{0} & {}^*\mathbf{U}_{2i}^{l+1} \end{bmatrix} \begin{bmatrix} \mathbf{0} & \mathbf{V}_{2i-1}^{l+1} \\ \mathbf{V}_{2i}^{l+1} & \mathbf{0} \end{bmatrix} = \mathbf{I} + \mathbf{U}_i^l\mathbf{V}_i^l \tag{19}$$

where $\mathbf{U}_i^l = \begin{bmatrix} {}^*\mathbf{U}_{2i-1}^{l+1} & \mathbf{0} \\ \mathbf{0} & {}^*\mathbf{U}_{2i}^{l+1} \end{bmatrix}$ and $\mathbf{V}_i^l = \begin{bmatrix} \mathbf{0} & \mathbf{V}_{2i-1}^{l+1} \\ \mathbf{V}_{2i}^{l+1} & \mathbf{0} \end{bmatrix}$. The asterisk on ${}^*\mathbf{U}_{2i-1}^{l+1}$, ${}^*\mathbf{U}_{2i}^{l+1}$ indicates the update of $\mathbf{U}_{2i-1}^{l+1}$, $\mathbf{U}_{2i}^{l+1}$ after factoring out ${}^*\mathbf{K}_{2i-1}^{l+1}$, ${}^*\mathbf{K}_{2i}^{l+1}$. This type of matrix can be readily inverted by using the Sherman-Morrison-Woodbury (SMW) formula [29,30]:

$$\left(\mathbf{I} + \mathbf{U}_i^l\mathbf{V}_i^l\right)^{-1} = \mathbf{I} - \mathbf{U}_i^l\left(\mathbf{I} + \mathbf{V}_i^l\mathbf{U}_i^l\right)^{-1}\mathbf{V}_i^l \tag{20}$$

Instead of using LU decomposition to invert the larger matrix on the left-hand side of Eq. (20) directly, SMW can be applied to invert a smaller matrix on the right-hand side, greatly reducing the computational cost, when the dimension N_i^l of $\mathbf{U}_i^l$ and $\mathbf{V}_i^l$ is much larger than the dimension p_i^l.

Then the key is how to decompose those off-diagonal submatrices into $\mathbf{U}_i^l\mathbf{V}_i^l$. To obtain the required decomposition, a fast and accurate algorithm is needed. For example, ACA has been used to approximate all off-diagonal submatrices in a HODLR matrix for solving 2D electromagnetic wave scattering BEM equations [21]. However, ACA is accurate only when two clusters are well separated geometrically, which is also named admissible. The hierarchically divided clusters usually do not satisfy the admissible condition in the top few tree levels. In this case, the randomized interpolative decomposition (ID) is a more accurate algorithm for the approximation.

To factorize an $m \times n$ matrix $\mathbf{A}$ with low-rank matrices, the most basic randomized algorithm starts from a $n \times k$ random test matrix $\boldsymbol{\Omega}$,

where $k < n$, of which every entry is an independent Gaussian random variable with a mean of 0 and a variance of 1. The multiplication of A and $\boldsymbol{\Omega}$, that is, $\mathbf{Y} = \mathbf{A}\boldsymbol{\Omega}$, forms a matrix in which each column of $\mathbf{Y}$ is a random sample in the range space of $\mathbf{A}$. The orthonormalized $\mathbf{Y}$ is a $m \times k$ matrix denoted as $\mathbf{Q}$ whose columns form the basis for the reduced column space of $\mathbf{A}$ [31]. Then the Row ID algorithm is applied to obtain the decomposition, which is presented as:

$$\mathbf{Q} = \mathbf{X}\mathbf{Q}_{(I,:)} \tag{21}$$

where the I is a set that contains indexes of k rows that span the row space of $\mathbf{Q}$. Thus $\mathbf{Q}_{(I,:)}$ denotes the subset of rows in $\mathbf{Q}$, and $\mathbf{X}$ is an $m \times k$ matrix containing an identity submatrix $\mathbf{X}_{(I,:)} = \mathbf{I}_k$. Furthermore, no entry of $\mathbf{X}$ is larger than 2 (or another reasonable small positive value).

After obtaining I and $\mathbf{X}$, we have:

$$\| \mathbf{A}_{m\times n} - \mathbf{X}_{m\times k}\mathbf{A}_{(I,:)k\times n}\| \leq \varepsilon \tag{22}$$

where $\| \cdot \|$ denotes the L2 operator norm. We would like k to be as small as possible for a given error tolerance ε of randomized ID, which means we want a better approximation with less use of core memory. The randomized algorithm is an effective aid to classical techniques. Considering the calculation of leverage scores for each row of $\mathbf{A}$ to decide whether to pick in ID as the second step, the randomize algorithm is the key of finding a subspace whose columns capture the action of column space of $\mathbf{A}$. Instead of forming an ID directly of $\mathbf{A}$, forming an ID of the sample matrix $\mathbf{Q}$ can reduce the overall computation cost, especially if the matrix is large. The random ID algorithm used here is based on an open-source code from P.G. Martinsson's research website [32], whose team has been working on various fast direct solvers for decades.

4. Algorithms

Applying all the formulations and matrix operations discussed above, the algorithm of the developed fast direct solver for the 3D acoustic BEM can be described as follows.

1) Read in the BEM model and construct a binary tree structure for the BEM matrix by hierarchically dividing the clusters. The information of the tree structure and the serial numbers of elements in each cluster are stored. The clusters at the lowest level of the tree structure are called leaves. By inputting the maximum number of elements allowed in a leaf as an initial parameter, the number of levels is determined correspondingly.
2) Construct the HODLR matrix and the right-hand-side (RHS) vector downward. From the top to every subsequential level of the tree structure, calculate the coefficients in the off-diagonal blocks of BEM matrix and the corresponding RHS vector. Use the randomized ID algorithm to update and store $\mathbf{U}$ and $\mathbf{V}$ of decomposed off-diagonal blocks, and use ACA for admissible blocks where appropriate. Down to the lowest level, the coefficients in the diagonal blocks of BEM matrix are calculated and stored directly. And through the contribution of the submatrices at each level, the RHS vector is continuously accumulated and finally formed.
3) Solve the HODLR matrix function by inverting submatrices upward. The unknown vector $\mathbf{x}$ on the boundary is solved as $\mathbf{x} = \mathbf{K}_0^{-1}\cdots\mathbf{K}_{l_m-1}^{-1}\mathbf{K}_{l_m}^{-1}\mathbf{b}$, in which $\mathbf{K}_{l_m}$ is a diagonal matrix and can be inverted directly. From the l_{m-1} level to every upper level, the diagonal blocks have the form of $\mathbf{I} + \mathbf{UV}$. The SMW formula algorithm is used to quickly invert these block diagonal matrices. Multiply the inverse of block diagonal matrices to RHS vector $\mathbf{b}$ and the $\mathbf{U}$ matrices for upper-level submatrices until reaching the top level.

5. Numerical examples

In this paper, all calculations are carried out using a computer with Intel Xeon 2.60GHz dual core CPUs and 128Gb RAM. Two examples with analytical solutions are solved first to verify the accuracy and efficiency of the method. Then, BEM models with more complicated geometries are considered.

5.1. Wave scattering from a rigid sphere

Consider a rigid sphere impinged upon by a plane incident wave. Assume the center of the sphere is located at the origin and has radius R, and the plane wave is incident along the positive x direction. In the spherical coordinate (r, θ, φ), the scattered pressure field can be expressed as:

$$p_s(r,\theta,\varphi) = -p_{0i}(\omega)\sum_{l=0}^{\infty}(2l+1)i^l\frac{j_l'(k_0a)}{h_l'^{(1)}(k_0a)}h_l^{(1)}(k_0r)P_l(\cos\theta) \tag{23}$$

where $p_{0i}(\omega)$ is the amplitude of the incident pressure wave, j_l and $h_l^{(1)}$ are spherical Bessel functions of the first kind and third kind (also named as Hankel function), respectively, and $P_l(\cos\theta)$ is the Legendre polynomials.

For the BEM model, 1200 to 86700 constant triangular elements are used to discretize the boundary of the sphere (with $R = 1$) for cases with the frequency ranging from 27.3Hz to 1856.1Hz. The corresponding wave number in these cases ranges from $k = 0.5$ to $k = 34$. The tolerance for the error in the randomized ID used is from $\varepsilon = 10^{-3}$ to $\varepsilon = 10^{-2}$. The representable mesh and wave scattering pressure contour is shown in Fig. 1.

Fig. 2 plots the numerical errors of the BEM solutions as compared with the analytical solutions at various different dimensionless wavenumber ka (with $a = 2R$ in this case). Results obtained using two different tolerance values are presented. The error is measured in its L2 norm, which is defined as:

$$\text{L2error} = \sqrt{\frac{\sum \| \mathrm{X}_{numerical} - \mathrm{X}_{analytical} \|^2}{\sum \| \mathrm{X}_{analytical} \|^2}} \tag{24}$$

From the Fig. 2, it is clear that without the Burton-Miller formulation, the error in the conventional BIE (CBIE) solutions peaks near the fictitious eigenfrequencies. Besides, the tolerance ε of randomized ID also affect the accuracy of the solution. When a tolerance of $\varepsilon = 10^{-3}$ is used, the error is less than 1%. Higher accuracy always requires longer calculation time. So, for most engineering applications, the $\varepsilon = 10^{-3}$ condition are likely to be sufficient to produce a reasonable accurate result with high efficiency. Compared to FMM BEM which needs to manually increase the number of multipole kernel expansion terms in the high frequency range, the set tolerance of ID helps to keep the desired accuracy automatically.

Fig. 3 shows the improvement on the computing time compared with the conventional direct BEM. And in this case, the ACA is applied for the admissible blocks with the admissible condition value η of 0.5, and the error still kept below 1%. The η is defined as:

$$\eta = \frac{\min\{diamt, diams\}}{dist(t,s)} \tag{25}$$

where t and s are two clusters; *diam* represents the diameter of clusters and *dist* is the distance of the centers of the two clusters. Since the fast direct solver has some extra setup, the saving of the fast direct solver starts when the number of elements is above around 10,000.

In the conventional BEM, constructing the matrix requires $O(N^2)$ operations and its solution via a direct approach requires $O(N^3)$ operations without parallel computing. The total complexity for the sphere case is around $O(N^{2.7})$, as shown in the trend line, which is well within the expected range. In HODLR based fast direct BEM, the complexity of constructing and storing a HODLR matrix is at most $O(N^2\log k)$ [33], where k is the rank of approximated matrix. It is affected by the settings in randomized ID and ACA, such as the rank of matrix when it finally

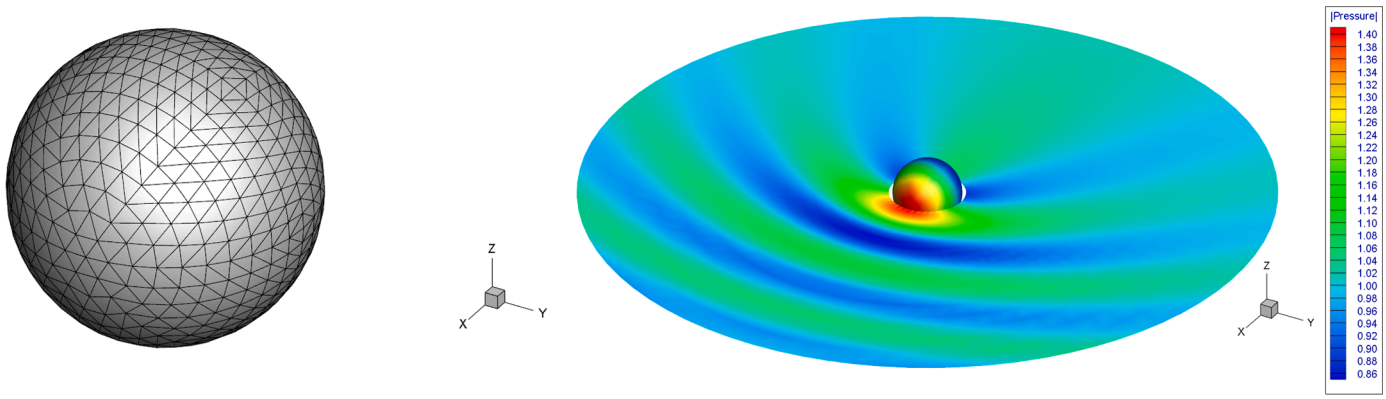

Fig. 1. Schematic illustration of a sphere corresponding to a plane wave incident along *-x* direction at 54.59Hz. The BEM mesh is shown in the left figure and the sound pressure contour is plotted in the right figure.

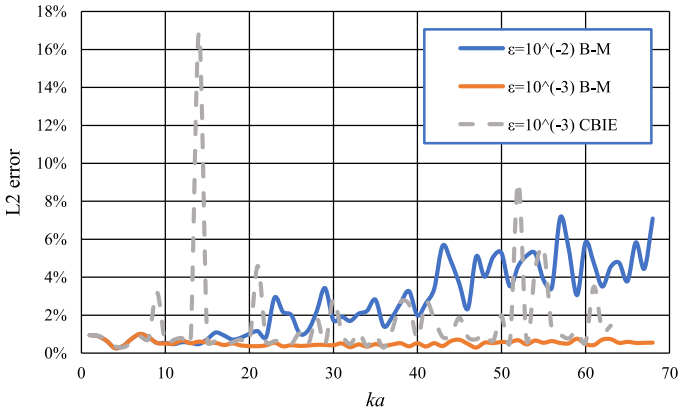

Fig. 2. L2 errors of pressure in the sphere scattering problem obtained from Burton-Miller (B-M) formulation and conventional boundary integral formulation (CBIE) with different randomized ID tolerance.

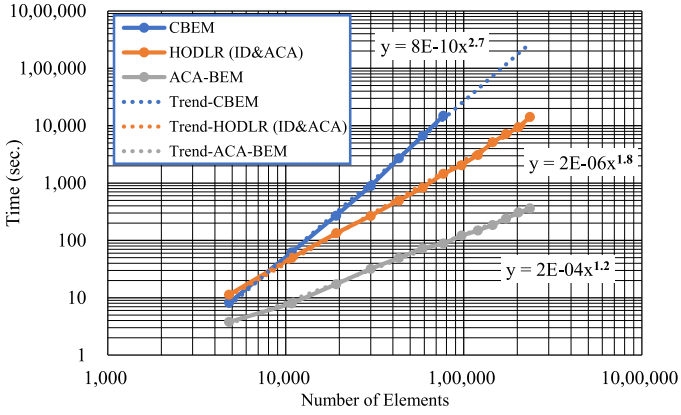

Fig. 3. Comparison of the CPU times with the conventional BEM, HODLR based fast direct BEM and ACA BEM for the sphere scattering problem with the wavenumber of 1.

achieves the required precision. And the cost of algorithm for factorization and inverse is $O(N\log^2 N)$ [18]. In this sphere scattering problem, the slope of the fast direct solver trend line indicates that the total complexity is actually close to $O(N^{1.8})$, which is a significant reduction from $O(N^{2.7})$ of the conventional BEM. For the largest model that can be solved by the conventional BEM solver, the total solution time is about 10 times of that using the new fast direct solver. In addition, the conventional BEM solver can only solve the model with the number of elements within 80,000 on the computer with 128Gb RAM, while the fast direct BEM solver can handle more than 240,000 elements on the same computer with the error below 1%. For comparison, the ACA solver in *FastBEM Acoustics*® software is also applied, which uses an iterative solver with the adaptive cross approximations in solving the BEM system of equations. The solution time of the iterative solver-based ACA BEM are also plotted in Fig. 3. It is seen that in this low-frequency case, the ACA solver has a complexity of $O(N^{1.2})$ and is faster than the new fast direct solver.

5.2. An interior acoustic problem

To further demonstrate the accuracy of the developed algorithm, an interior acoustic problem with known exact solution is considered. Room acoustics is a subject that has received widespread attention and is closely related to everyday life. The simple testing case considered here is an enclosed cuboid with an inside point source. The pressure field inside the cuboid can be expressed as a linear combination of eigenfunctions satisfying the Helmholtz equation:

$$p = \sum_n A_n \Psi(\mathbf{x}, n) \tag{26}$$

The eigen-functions and eigenvalues k_n can be derived as:

$$\Psi(\mathbf{x}, n_x, n_y, n_z) = \cos\left(\frac{n_x\pi}{L_x}x\right)\cos\left(\frac{n_y\pi}{L_y}y\right)\cos\left(\frac{n_z\pi}{L_z}z\right) \tag{27}$$

$$k_n^2 = \left(\frac{n_x\pi}{L_x}\right)^2 + \left(\frac{n_y\pi}{L_y}\right)^2 + \left(\frac{n_z\pi}{L_z}\right)^2 \tag{28}$$

A_n is the mode participation coefficient given by:

$$A_n = q_n \frac{\varpi}{V\left[k^2 - k_n^2\right]}\cos\left(\frac{n_x\pi}{L_x}x_s\right)\cos\left(\frac{n_y\pi}{L_y}y_s\right)\cos\left(\frac{n_z\pi}{L_z}z_s\right) \tag{29}$$

where L_x,L_y,L_z are dimensions of the room, x_s,y_s,z_s are the coordinates of the source location, ϖ is the source strength, and $q_n = q_x(n_x)q_y(n_y)q_z(n_z)$ ($q_x(n_x) = 1$ for $n_x = 0$ and $q_x(n_x) = 2$ for $n_x \neq 0$). Similar conditions are applied to q_y and q_z as well. One model with edge lengths of $L_x = 1$, $L_y = 1$, $L_z = 0.5$ is presented in Fig. 4. There are a total of 7200 elements in this model and the point source is located at (0.8, 0.8, 0.4).

With a tolerance of $\varepsilon = 10^{-3}$, cuboids with different aspect ratios are simulated by the HODLR based fast direct BEM. There are 10 models with the same edge length $L_x = L_y = 1$ in both x and y directions, and the edge length in the z direction ranging from $L_z = 0.1$ to $L_z = 1$. In all models, the point source is located at (0.5, 0.5, 0.05) and the evaluation point is located at (0.1, 0.1, 0.05). The element size and rigid boundary faces are all the same. The frequency studied ranges from 60 to 150Hz

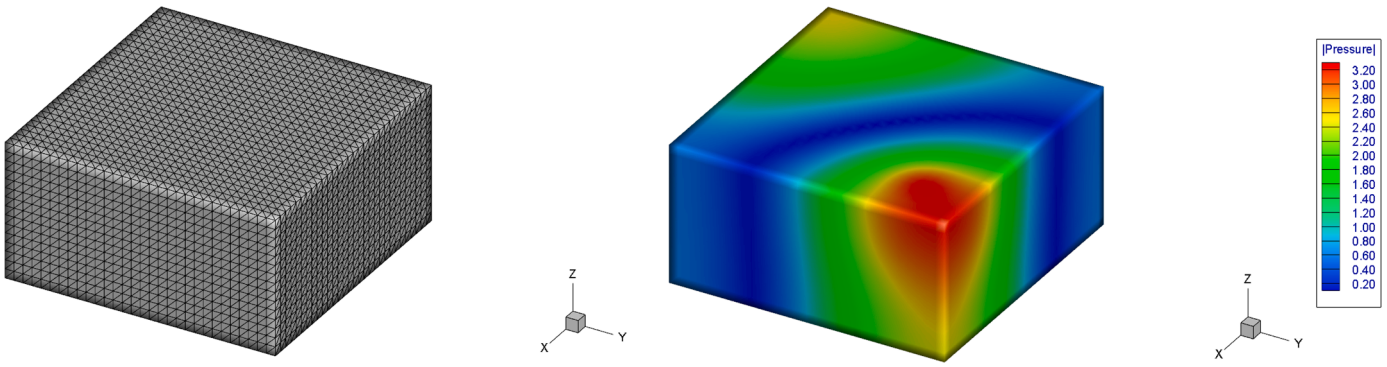

Fig. 4. Schematic illustration of a cuboid with a point sound source located at (0.8, 0.8, 0.4). The edge lengths of the cuboid in this figure are $L_x = 1$, $L_y = 1$, $L_z = 0.5$ respectively, and the frequency of the sound source is 150Hz. The BEM mesh is shown in the left figure and the sound pressure contour is plotted in the right figure.

with an interval of 10Hz. The average L2 error of the pressure at the evaluation point over the 10 frequencies for each model is shown in Table 1. The results in Table 1. indicate that the fast direct solver can deal with the internal problems of different aspect ratios accurately. The error remains very small when the aspect ratio is as low as 1/10.

Regarding the efficiency, the CPU time is recorded in a frequency sweep study for the cube model with 10800 elements and shown in Fig. 5. As can be seen in the figure, the CPU time increases with the frequency slightly. The increase in time mainly come from two parts: the randomized ID approximation and the SMW formula matrix inversion. In the high frequency range, the coefficient matrix represents the action of highly oscillatory integral kernels. As stated earlier, the randomized algorithm is used to formulate a subspace that represents well the column space of coefficient matrix. In order to capture all oscillations, the randomized algorithm takes longer to sample as the frequency increases. The approximated submatrices $\mathbf{U}_i^l$ and $\mathbf{V}_i^l$ are larger, and the efficiency of SMW formula is reduced accordingly. Although the computation time increases a bit with the frequency, this is much less severe compared to the cases with the fast BEM using iterative solvers, such as the ACA BEM also shown in the figure. The advantage in the solution speed is lost for the ACA BEM in the higher frequency ranges. Therefore, the HODLR based fast direct solver has unique advantages in the broadband simulation.

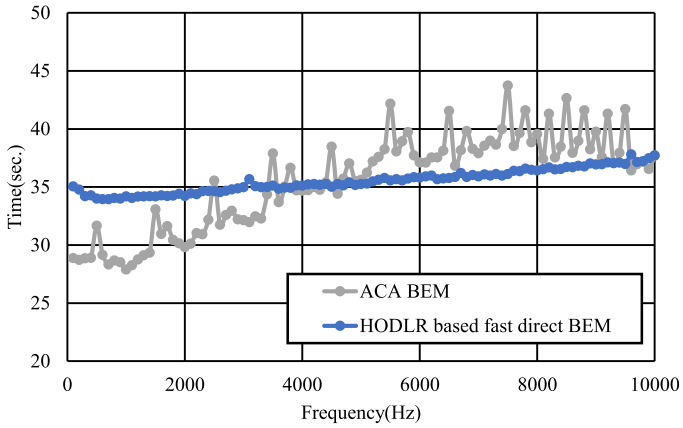

Fig. 5. CPU time of the HODLR based fast direct BEM and ACA BEM for the room acoustic model as a function of frequency. The number of elements is 10800.

5.3. Torus arrays

A modern approach to control sound is through the development of sound-control structures, which can produce a specific wavefront when they are illuminated with a suitable coherent source. For example, phononic crystals are artificial composite materials consisting of periodical arrangement of identical structures. Controlling the material composition, structure topology and size leads to different acoustic bandgaps and thus different sound control performance. A torus array is simulated here to demonstrate the capability of the fast direct solver on handling wave scattering problems with multiple objects.

The geometry of a torus and an array of nine tori are illustrated in Fig. 6. Each torus has a tube radius of $r = 0.05$ and a torus radius of $R = 0.13$, and the distance between each two torus is $d = 0.025$. The center of array is located at the origin, and all tori are distributed uniformly on the y-z plane around the center. A plane wave is incident along the $-x$ axis. If the incident wavelength is greater than the hollow diameter of the torus, the scattered pressure field of the torus is similar to that of a sphere with the same characteristic length. The difference begins to manifest as the wavelength decreases below the hollow diameter of $R - r$. Two models with 3×3 torus array and 5×5 torus array are studied for a frequency range of [500, 5500]Hz. The sound pressure at an evaluation point (-5,0,0) located on the transmitted wave side is plotted in Fig. 7.

In both models, it is observed that there is an extreme low-pressure value with the magnitude of around 0.1 occurring around the frequency of 4350Hz and 5000Hz for the 3×3 and 5×5 arrays respectively. To investigate whether there is a quiet region at these two special frequencies, the sound pressure in a region behind the array is plotted in Fig. 8. There is indeed a quiet region in both cases, which is likely formed due to the destructive interference between the wave passing

Table 1
L2 error of the pressure at the evaluation point inside an enclosed cuboid with an interior point source, averaged from 60 to 150Hz.

X-length	Y-length	Z-length	DOFs	L2 error
1	1	1	10800	0.207%
1	1	0.9	10080	0.213%
1	1	0.8	9360	0.244%
1	1	0.7	8640	0.179%
1	1	0.6	7920	0.263%
1	1	0.5	7200	0.221%
1	1	0.4	6480	0.188%
1	1	0.3	5760	0.250%
1	1	0.2	5040	0.195%
1	1	0.1	4320	0.114%

Table 2
The number of elements and simulation time of each stage of the Menger structures at the frequency of 1000Hz.

Menger Structure	Stage 1	Stage 2	Stage 3
Number of Elements	9804	16192	56876
Time (sec.)	28.64	118.67	754.89

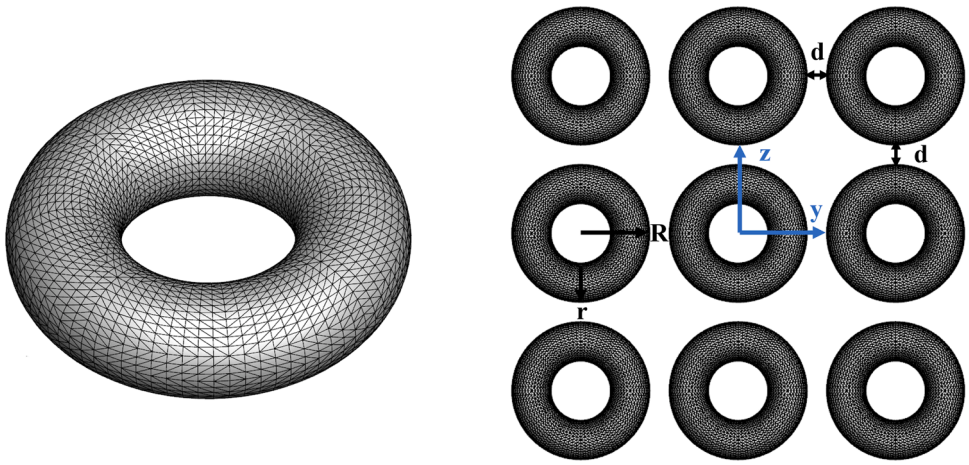

Fig. 6. Schematic of the geometry and the mesh of a single torus (left) and an array (right)

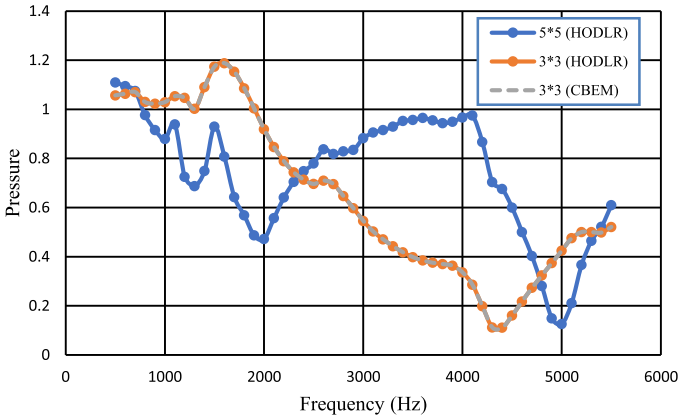

Fig. 7. Sound pressure of the point located at (-5,0,0) at different frequencies in the two models obtained from the conventional direct BEM solver and the fast direct solver.

directly through the orifice and the scattered wave from the curved surface of the torus. This phenomenon has also been observed in other types of metamaterials such as perforated plate [34], the resonator array with central hole [35], and metamaterial with unit cells contain central hollow and surrounding helix structure [36,37].

As shown in Fig. 7, the results obtained from the conventional BEM match well with those obtained from the fast direct solver in the model with 3×3 torus array indicating the accuracy of the fast direct solver. However, the total CPU time taken by the conventional solver is two days longer than that of the fast direct solver. As for the 5×5 array model, the required memory is too large for the conventional BEM solver. The swept frequency calculation of the 25-torus array model can be finished within 16 hours, with the parallel calculation of the discretized kernel integration. Another approach to significantly cut the CPU time for frequency sweep calculation is to employ the model-order reduction method for the acoustic BEM [38].

5.4. Menger fractal structures

Menger structures are fractals constructed hierarchically as illustrated in Fig. 9. There are two types of Menger fractal structures: the convex form and the concave form. Researchers have studied their acoustic properties and found that both could be regarded as acoustic metamaterials with negative refraction and sound absorption capability [39,40]. The concave structure is also called Menger sponge. According to the Ref. [39], the sound absorption capabilities of the first and the second stage Menger spongers were analyzed experimentally and theoretically. It was found that although the absorption magnitudes of the two types of structures were quite different, the trends of the sound absorption coefficient as a function of the frequency in the two cases were similar.

As another validation case with a complex domain, it would be interesting to simulate the sound absorption of Menger structures using the fast direct solver. Since the specific parameters of sound impedance tube experiment are not specified in the Ref. [39], a similar case is simulated here. The absorption coefficient α is defined as:

$$\alpha = 1 - \left| \frac{H_{12} - e^{-iks}}{e^{iks} - H_{12}} \right|^2 \tag{30}$$

where $H_{12} = p(x_2)/p(x_1)$ is the ratio of the acoustic pressures at two testing points located on the inner wall of impedance tube as shown in Fig. 10(a), k is the wavenumber, and s is the distance between the two test points. The rectangular tube with a length of $1.35m$ and a cross section area of $0.3 \times 0.3m^2$ is modeled using the hard-wall condition.

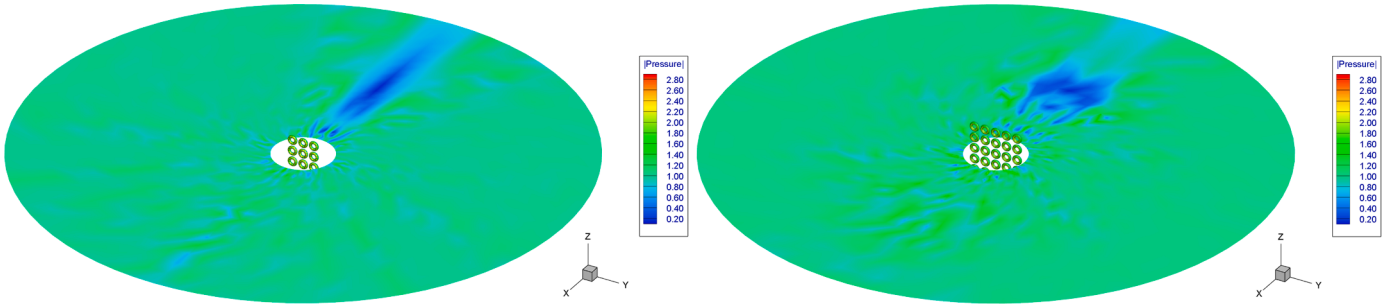

Fig. 8. Sound pressure field contour plot of 3×3 torus array at 4350Hz (left) and 5×5 torus array at 5000Hz (right).

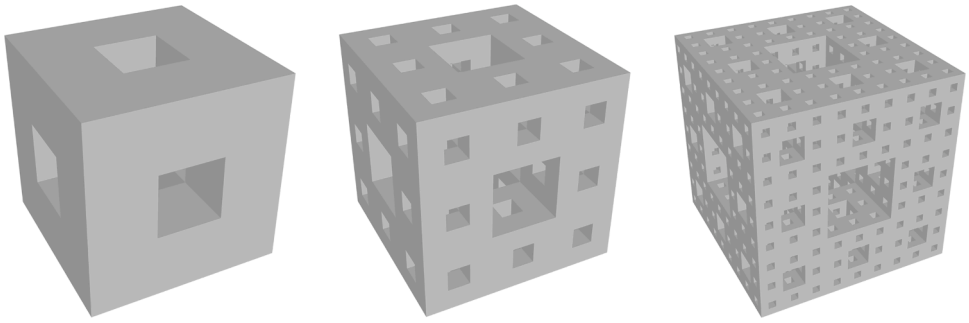

Fig. 9. Illustration of concave Menger structures of different stages: stage 1, stage 2, and stage 3 (from left to right).

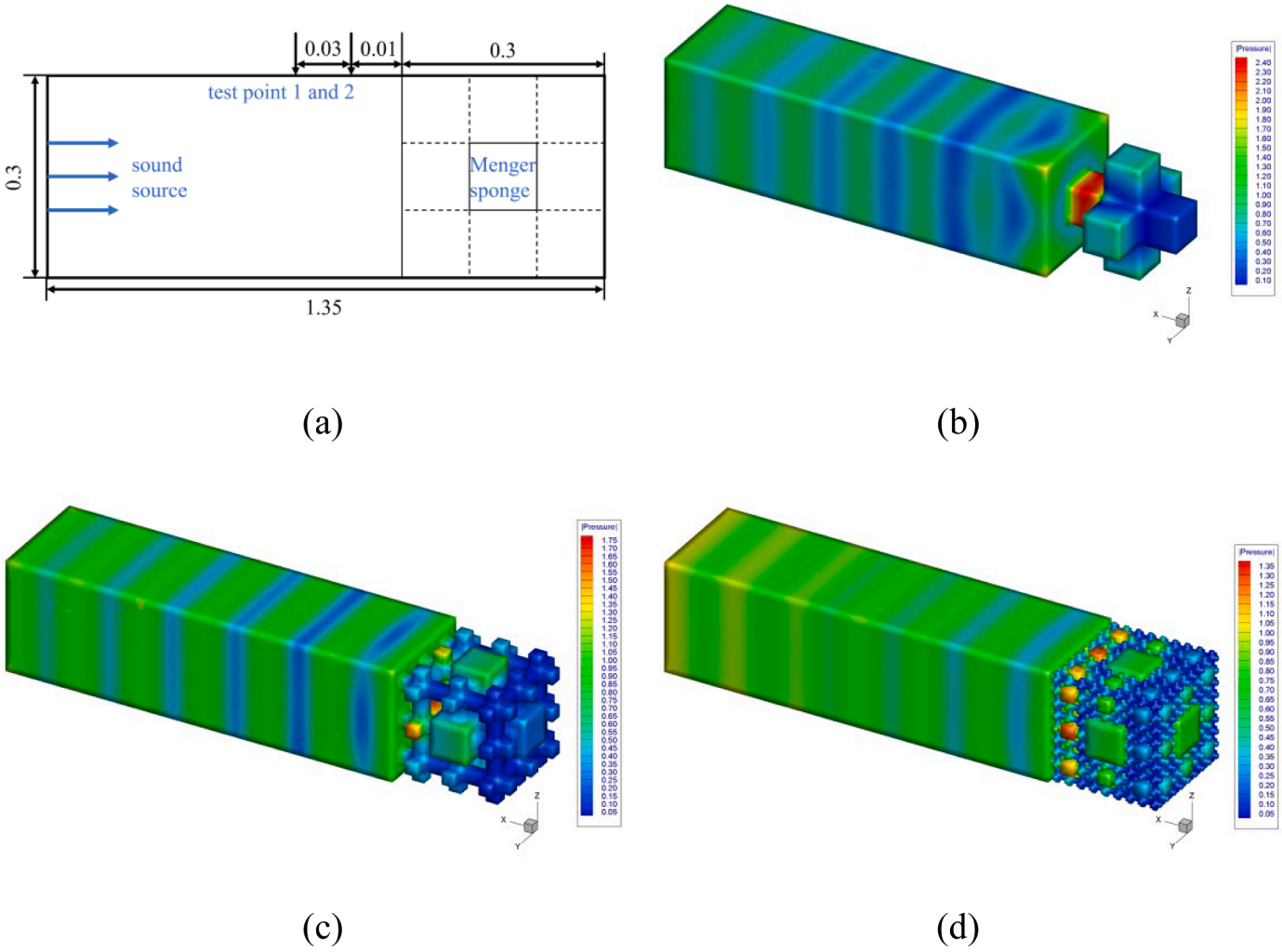

Fig. 10. (a) Schematic of the simulation model; The total sound pressure field inside Menger structures at 1000Hz: (b) stage 1, (c) stage 2 and (d) stage 3.

The two testing points are located $0.01m$ and $0.04m$ away from the Menger sponge respectively. A plane pressure wave is incident from the left end of the tube and the Menger structure is located on the right end of the tube as shown in Fig. 10(a). The frequency range studied is from 400Hz to 1400Hz. The simulated total sound pressures in three cases corresponding to the three stages are plotted in Fig. 10 (b), (c) and (d) respectively. For clarity, solid structures are not shown and only sound pressure inside the air cavities of the structure is shown.

The simulated sound absorption coefficients at different frequencies are plotted in Fig. 11. The overall trends of the absorption coefficient in stage 1 and stage 2 are consistent with the experimental results presented by Kawabe et al. [39], that is, the absorption coefficient exhibits a peak at a particular frequency, indicating a resonance behavior. When the structure changes from stage 1 to stage 2, the peak decreases and but the average absorption coefficient increases, suggesting that more cavities participate in sound absorption. Such an absorption mechanism becomes more dominate when the structure changes to stage 3. As shown in Fig. 11, the absorption coefficient becomes more broadband with an increased average value and less prominent peaks. The maximum value of the absorption coefficient, however, does not decrease further, but rises to almost the same level as that of the first stage. Overall, the third stage Menger sponge exhibits significantly

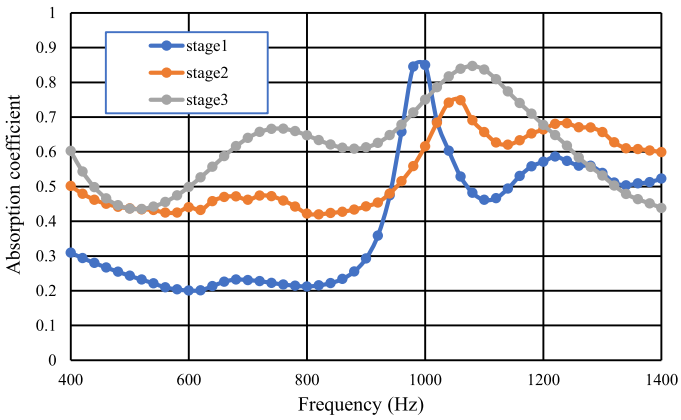

Fig. 11. Sound absorption coefficients of the three Menger sponges as functions of the frequency.

better sound absorption capability than the first and the second stage models within the considered frequency range. As for the computational efficiency, the simulation over the entire frequency range is finished within 15 hours on the workstation in all three structures (Table 2).

6. Discussions

In this paper, a HODLR based fast direct BEM for solving 3D acoustic problems is presented. The formulation of acoustic BEM is reviewed, and the construction, decomposition, approximation and inversion of the HODLR matrix in the BEM are provided. Several numerical examples are used to demonstrate the performance of the fast solver. It has been verified that the HODLR based fast direct BEM solver can accurately and efficiently solve both scattering problems and interior acoustic problems. The results show significant advantages in CPU time and memory usage compared to the conventional direct BEM.

The HODLR based fast direct solver also has some distinct properties in comparison with other fast BEMs. The FMM BEM requires adjustment to the number of expansion terms to maintain the accuracy as the frequency becomes higher, whereas the HODLR based fast direct BEM has a fixed approximation tolerance over the entire frequency range. The rank of approximated submatrices automatically increases with frequency to obtain high accuracy. And secondly, the number of iterations required in iterative solver based fast methods usually increases with the frequency, which will result in significantly increased CPU time. In contrast, the computation efficiency of fast direct BEM is only slightly affected by the frequency. Even though in some cases the iterative solver based fast BEM algorithms are more efficient in memory usage and CPU time, the fast direct BEM algorithms are overall more stable with predictable errors, memory usage and CPU time requirement.

To improve the computational efficiency of the developed fast direct solver, several techniques can be applied. Firstly, applying multi-threaded parallelism to the partitioned submatrices will save the computation time, while it requires higher core memory during computation process. It is efficient to calculate submatrices at the same level simultaneously, since they are independent to each other. Secondly, the adaptive strategy can improve the matrix division. The fewer the layers, the shorter the time of ID algorithm and the longer the time of SMW matrix inverse algorithm. Therefore, the size of submatrices at the lowest level can be decided adaptively to achieve the highest efficiency. In addition, the recently emerged machine learning-based low-rank approximation algorithm [41] could potentially be a suitable choice to further improve the efficiency of the fast direct BEM solvers. These techniques can be studied and implemented in order to further improve the fast direct BEM solver.

Declaration of Competing Interest

The authors declare the following financial interests/personal relationships which may be considered as potential competing interests:

Yijun Liu reports financial support was provided by National Natural Science Foundation of China (Project No. 11972179). Liu and Ye are serving as the guest editors for this special issue and thus would like to request the chief editor (Dr. Cheng) to assign the reviewers for this paper.

Data availability

Data will be made available on request.

Acknowledgement

The authors would like to thank the financial support to this work from the National Natural Science Foundation of China (Project No. 11972179).

References

[1] Burton AJ, Miller GF. The application of integral equation methods to the numerical solution of some exterior boundary-value problems. Proc R Soc London, Ser A 1971;323:201–10.
[2] Liu YJ. On the BEM for acoustic wave problems. Eng Anal Boundary Elem 2019;107:53–62.
[3] Zheng C-J, Chen H-B, Gao H-F, Du L. Is the Burton–Miller formulation really free of fictitious eigenfrequencies? Eng Anal Boundary Elem 2015;59(0):43–51.
[4] Martinez R. The thin-shape breakdown (TSB) of the Helmholtz integral equation. J Acoust Soc Am 1991;90(5):2728–38.
[5] Liu YJ, Rizzo FJ. Scattering of elastic waves from thin shapes in three dimensions using the composite boundary integral equation formulation. J Acoust Soc Am 1997;102(2):926–32 (Pt.1, August).
[6] Rokhlin V. Rapid solution of integral equations of scattering theory in two dimensions. J Comput Phys 1990;86(2):414–39.
[7] Rokhlin V. Diagonal forms of translation operators for the Helmholtz equation in three dimensions. Appl Comput Harmon Anal 1993;1(1):82–93.
[8] Hackbusch W. A sparse matrix arithmetic based on $\mathscr{H}$-matrices. Part I: Introduction to $\mathscr{H}$-matrices. Computing 1999;62(2):89–108.
[9] Liu YJ. Fast multipole boundary element method - theory and applications in engineering. Cambridge: Cambridge University Press; 2009.
[10] Nishimura N. Fast multipole accelerated boundary integral equation methods. Appl Mech Rev 2002;55(4):299–324 (July).
[11] Liu YJ, Nishimura N. The fast multipole boundary element method for potential problems: a tutorial. Eng Anal Bound Elem 2006;30(5):371–81.
[12] Liu YJ, Mukherjee S, Nishimura N, Schanz M, Ye W, Sutradhar A, et al. Recent advances and emerging applications of the boundary element method. Appl Mech Rev 2012;64(March):1–38.
[13] Bebendorf M. Approximation of boundary element matrices. Numer Math 2000;86(4):565–89.
[14] Rjasanow S, Steinbach O. The fast solution of boundary integral equations. Berlin: Springer; 2007.
[15] Bebendorf M. Hierarchical matrices: a means to efficiently solve elliptic boundary value problems. Berlin: Springer-Verlag; 2008.
[16] Brancati A, Aliabadi MH, Benedetti I. Hierarchical adaptive cross approximation GMRES technique for solution of acoustic problems using the boundary element method. CMES: Comput Model Eng Sci 2009;43(2):149–72.
[17] Saad Y, Schultz M. A generalized minimal residual algorithm for solving nonsymmetric linear system. SIAM J Stat Comp 1986;7:856–69.
[18] Ambikasaran S, Darve E. An $O(N\log N)$ fast direct solver for partial hierarchically semi-separable matrices. J Sci Comput 2013;57(3):477–501.
[19] Kong WY, Bremer J, Rokhlin V. An adaptive fast direct solver for boundary integral equations in two dimensions. Appl Comput Harmon Anal 2011;31(3):346–69.
[20] Bebendorf M. Hierarchical LU decomposition-based preconditioners for BEM. Computing 2005;74(3):225–47.
[21] Lai J, Ambikasaran S, Greengard L. A fast direct solver for high frequency scattering from a large cavity in two dimensions. SIAM J Sci Comput 2014;36(6):887–903.
[22] Borges C, Greengard L. Inverse obstacle scattering in two dimensions with multiple frequency data and multiple angles of incidence. SIAM J Imag Sci 2015;8(1):280–98.
[23] Liberty E, Woolfe F, Martinsson P-G, Rokhlin V, Tygert M. Randomized algorithms for the low-rank approximation of matrices. Proc Natl Acad Sci 2007;104(51):20167–72.
[24] Martinsson P-G, Rokhlin V, Tygert M. A randomized algorithm for the decomposition of matrices. Appl Comput Harmon Anal 2011;30(1):47–68.

[25] Huang S, Liu YJ. A new fast direct solver for the boundary element method. Comput Mech 2017;60(3):379–92.
[26] Sun FL, Dong CY, Wu YH, Gong YP. Fast direct isogeometric boundary element method for 3D potential problems based on HODLR matrix. Appl Math Comput 2019;359:17–33.
[27] Liu YJ, Rizzo FJ. A weakly-singular form of the hypersingular boundary integral equation applied to 3-D acoustic wave problems. Comput Meth Appl Mech Eng 1992;96:271–87.
[28] Ambikasaran S. Fast algorithms for dense numerical linear algebra and applications. Stanford University; 2013.
[29] Sherman J, Morrison WJ. Adjustment of an inverse matrix corresponding to a change in one element of a given matrix. Annal Math Statist 1950;21(1):124–7.
[30] Woodbury MA. Inverting modified matrices: Statistical Research Group; 1950.
[31] Halko N, Martinsson P-G, Tropp JA. Finding structure with randomness: probabilistic algorithms for constructing approximate matrix decompositions. SIAM Rev 2011;53(2):217–88.
[32] Tygert M, Martinsson P-G, Rokhlin V, Shkolnisky Y.ID. https://users.oden.utexas.edu/~pgm/main_codes.
[33] Martinsson P-G, Tropp JA. Randomized numerical linear algebra: foundations and algorithms. Acta Numer 2020;29:403–572.
[34] Wang X, Luo X, Yang B, Huang Z. Ultrathin and durable open metamaterials for simultaneous ventilation and sound reduction. Appl Phys Lett 2019;115(17):171902.
[35] Kim S-H, Lee S-H. Air transparent soundproof window. AIP Adv 2014;4(11):117123.
[36] Ghaffarivardavagh R, Nikolajczyk J, Anderson S, Zhang X. Ultra-open acoustic metamaterial silencer. J Acoust Soc Am 2019;145(3). 1726-26.
[37] Sun M, Fang X, Mao D, Wang X, Li Y. Broadband acoustic ventilation barriers. Phys Rev Appl 2020;13(4):044028.
[38] Xie X, Liu YJ. An adaptive model order reduction method for boundary element-based multi-frequency acoustic wave problems. Comput Meth Appl Mech Eng 2021;373:113532.
[39] Kawabe T, Miyazaki T, Oka D, Si Koyanagi, Hinokidani A. Sound absorption by Menger sponge fractal. J Acoust Soc Am 2009;125(5):2830–3.
[40] Liu Y, Xu W, Chen M, Pei D, Yang T, Jiang H, et al. Menger fractal structure with negative refraction and sound tunnelling properties. Mater Res Express 2019;6(11):116211.
[41] Indyk P, Vakilian A, Yuan Y. Learning-based low-rank approximations. arXiv preprint arXiv:191013984 2019.